

# Fault Detection for Aircraft Control Surfaces Using Approximate Input Reconstruction

Haoyun Fu<sup>1</sup>, Jin Yan<sup>1</sup>, Mario A. Santillo<sup>1</sup>, Harish J. Palanthandlam-Madapusi<sup>2</sup>, and Dennis S. Bernstein<sup>1</sup>

**Abstract**—We use an approximate input reconstruction algorithm to reconstruct unknown inputs, which are then used as a basis for fault detection. The approximate input reconstruction algorithm is a least squares algorithm that estimates both the unknown initial state and input history. The estimated inputs are then compared to the commanded values and sensor values to assess the health of actuators and sensors. This approach is applied to the longitudinal and lateral dynamics of an aircraft. The input reconstruction algorithm can be used for minimum-phase or nonminimum-phase zeros; however, zeros on the unit circle yield persistent estimation errors and thus poor input reconstruction.

## I. INTRODUCTION

As systems in general—and control systems in particular—become more complex, there is an increasing need to monitor critical components to ensure their proper operation. This problem is known generically as either *fault diagnosis* or *fault detection* [1–4].

A widely studied approach to fault detection is to use input observers to reconstruct inputs to the system based on an available system model and measurements. The estimated inputs can then be compared to expected inputs to assess the health of sensors and actuators. The relevant literature on this topic has its roots in system inversion theory developed for either input observers (left inversion) or preview control (right inversion) [5–15]. One of the difficulties in system inversion is the presence of zeros. If the system has no zeros, then input reconstruction is possible even if the initial state is zero [15]. However, if the system has zeros, then there exists an initial state such that, for some nonzero input, the output is identically zero. Therefore, exact input reconstruction is impossible if the system has at least one zero. For a minimum-phase zero, the unobservable input decays, and thus asymptotically input observation is possible. On the other hand, for a nonminimum-phase zero, the unobservable input increases without bound, and thus input observation is possible asymptotically backward in time, that is, noncausally for large data sets. As a consequence, if a system has a minimum-phase zero and a nonminimum-phase zero, then input reconstruction is possible for time steps that are neither large nor small. Finally, if the zero lies on the unit disk, then the unobservable input is persistent (non-decaying in either forward or backward time) and thus input reconstruction is not feasible.

This work was sponsored by NASA under IRAC grant NNX08AB92A and the Aerospace Engineering Department of the University of Michigan.

<sup>1</sup>Department of Aerospace Engineering, The University of Michigan, Ann Arbor, MI 48109, haoyunfu, yanjin, santillo, dsbaero@umich.edu

<sup>2</sup>Department of Mechanical and Aerospace Engineering, Syracuse University, Syracuse, NY 13244, h.j.palant@syr.edu

In the present paper we begin by reviewing the exact input reconstruction method developed in [15]. Since this approach assumes that the system has no zeros, we estimate the input by using a least squares solution of the input-output relation. The resulting estimate is unable to estimate input components in the null space of the coefficient matrix, which corresponds to the unobservable input component.

We apply this algorithm to the linearized longitudinal and lateral dynamics of an aircraft in order to estimate thrust inputs as well as control-surface deflections. These estimates can be used to detect faults in the actuator or linkage sensor associated with the control surface. We consider examples in which the dynamics are minimum phase and nonminimum phase, as well as strictly proper and exactly proper, the latter occurring when the measurement is given by an accelerometer.

## II. FAULTS IN AN AIRCRAFT DYNAMIC SYSTEM

We consider the aircraft elevator and engine subsystems, which can potentially undergo various faults. The elevator is assumed to have a local sensor, called the *linkage sensor*, which provides a measurement of the deflection of the linkage that drives the elevator. Consequently, the elevator subsystem can undergo various faults; for example, the control surface may be damaged, the linkage may be damaged, or the linkage sensor may malfunction.

Figure 1 shows the various signals that are used for fault diagnosis. Specifically,  $\delta e_{k,\text{com}}$  is the command to the elevator,  $\hat{\delta e}_k$  is the reconstructed (estimated) value of the elevator deflection, and  $l_{k,\text{msmt}}$  is the signal from the linkage sensor. As discussed below, discrepancies between these signals suggest the possibility of various types of failures.

Notation	Description
$\delta e_{k,\text{com}}$	commanded elevator input
$\delta e_{k,\text{act}}$	actual elevator output
$l_{k,\text{act}}$	actual linkage output
$l_{k,\text{msmt}}$	linkage sensor measurement
$\hat{\delta e}_k$	estimated elevator input
$\delta T_{k,\text{com}}$	commanded engine input
$\delta T_{k,\text{act}}$	actual engine output
$\delta T_{k,\text{msmt}}$	actual RPM sensor output
$\hat{\delta T}_k$	estimated engine input

TABLE I  
 NOTATION FOR SIGNALS USED TO IDENTIFY FAULTS

Linkage Sensor Fault	Description
Bias	$l_{k,\text{msmt}} = l_{k,\text{act}} + b$
Drift	$l_{k,\text{msmt}} = l_{k,\text{act}} + kc$
Frozen	$l_{k,\text{msmt}} = b$
Scale Factor Error	$l_{k,\text{msmt}} = l_{k,\text{act}}b$

TABLE II  
LINKAGE SENSOR FAULTS

Case	Condition	Linkage Sensor	Linkage	Elevator
1	$\delta e_{k,\text{com}} = \delta \hat{e}_k = l_{k,\text{msmt}}$	✓	✓	✓
2	$\delta e_{k,\text{com}} = \delta \hat{e}_k \neq l_{k,\text{msmt}}$	Faulty	✓	✓
3	$\delta e_{k,\text{com}} \neq \delta \hat{e}_k = l_{k,\text{msmt}}$	✓	Faulty	✓
4	$\delta e_{k,\text{com}} = l_{k,\text{msmt}} \neq \delta \hat{e}_k$	✓	✓	Faulty
5	$\delta e_{k,\text{com}} \neq \delta \hat{e}_k$ and $\delta e_{k,\text{com}} \neq l_{k,\text{msmt}}$	Combination of Cases 2, 3, 4		

TABLE III

FAULT DETECTION ANALYSIS FOR THE ELEVATOR

We consider the possibility that the linkage can fail in various ways. In particular, we consider linkage faults that include saturation, rate saturation, deadzone, and frozen. In addition, linkage sensor faults include bias, drift, frozen, and calibration error. These faults are listed in Table 2, where  $b$  is a constant and  $c$  is a positive number.

The elevator control surface can fail in various ways. For example, the elevator may become stuck in a single, fixed deflection. Alternatively, the elevator may become deformed or damaged, resulting in a loss of control effectiveness. Detection of these faults is relevant to health monitoring to avoid loss of control system performance.

For the elevator, we detect faults during flight by comparing the commanded inputs  $\delta e_{k,\text{com}}$ , the measured inputs from the linkage sensor  $l_{k,\text{msmt}}$ , and the estimated inputs from input reconstruction  $\delta \hat{e}_k$ . Table 3 shows the logic by which these signals are compared. For example, if the linkage measurement differs from the commanded elevator deflection and the estimation elevator deflection, then we can conclude that the linkage sensor is faulty but that the linkage and elevator are both operational. In practice, all of these signals are noisy, and thus error criteria are needed. For simplicity, Table 3 is stated in terms of equality and inequality of signals. A similar fault analysis can be applied to other control surfaces and the engine.

### III. INPUT RECONSTRUCTION

In this section, we briefly review the input reconstruction method developed in [15]. We consider both the strictly proper and exactly proper cases, which are used in later sections for numerical examples.

#### A. Strictly Proper Case

Consider the linear discrete-time system

$$x_{k+1} = Ax_k + He_k, \quad (\text{III.1})$$

$$y_k = Cx_k, \quad (\text{III.2})$$

where  $x_k \in \mathbb{R}^n$ ,  $e_k \in \mathbb{R}^p$ ,  $y_k \in \mathbb{R}^l$ ,  $A \in \mathbb{R}^{n \times n}$ ,  $H \in \mathbb{R}^{n \times p}$ , and  $C \in \mathbb{R}^{l \times n}$ . The input  $e_k$  and the initial state  $x_0$  are assumed to be unknown. Without loss of generality, we assume  $l \leq n$ ,  $\text{rank}(C) = l > 0$ , and  $\text{rank}(H) = p > 0$ . For a nonnegative integer  $r$ , define  $\mathcal{Y}_r \in \mathbb{R}^{(r+1)l}$  and  $\mathcal{E}_r \in \mathbb{R}^{(r+1)p}$

as

$$\mathcal{Y}_r \triangleq \begin{bmatrix} y_0 \\ y_1 \\ \vdots \\ y_r \end{bmatrix}, \quad \mathcal{E}_r \triangleq \begin{bmatrix} e_0 \\ e_1 \\ \vdots \\ e_r \end{bmatrix}. \quad (\text{III.3})$$

*Definition 3.1:* Let  $r \geq 1$ . Then the *input and state unobservable subspace*  $\mathfrak{U}_r$  of (III.1), (III.2) is the subspace

$$\mathfrak{U}_r \triangleq \left\{ \begin{bmatrix} x_0 \\ \mathcal{E}_{r-1} \end{bmatrix} \in \mathbb{R}^{n+rp} : \mathcal{Y}_r = 0 \right\}. \quad (\text{III.4})$$

*Definition 3.2:* The system (III.1), (III.2) is *input and state unobservable* if  $\mathfrak{U}_r = \{0\}$  for all  $r \geq r_0$ .

Define  $\Gamma_r \in \mathbb{R}^{(r+1)l \times n}$ ,  $M_r \in \mathbb{R}^{(r+1)l \times rp}$ , and  $\Psi_r \in \mathbb{R}^{(r+1)l \times (n+rp)}$  by

$$\Gamma_r \triangleq \begin{bmatrix} C \\ CA \\ CA^2 \\ \vdots \\ CA^r \end{bmatrix}, \quad M_r \triangleq \begin{bmatrix} 0 & 0 & \cdots & 0 \\ CH & 0 & \cdots & 0 \\ CAH & CH & \cdots & 0 \\ \vdots & \vdots & \ddots & \vdots \\ CA^{r-1}H & CA^{r-2}H & \cdots & CH \end{bmatrix},$$

and

$$\Psi_r \triangleq [\Gamma_r \ M_r]. \quad (\text{III.5})$$

Then from (III.1), (III.2), we can write

$$\mathcal{Y}_r = \Gamma_r x_0 + M_r \mathcal{E}_{r-1} = \Psi_r \begin{bmatrix} x_0 \\ \mathcal{E}_{r-1} \end{bmatrix}, \quad (\text{III.6})$$

so that

$$\mathfrak{U}_r = \mathcal{N}(\Psi_r), \quad (\text{III.7})$$

where  $\mathcal{N}$  denotes null space. Next, define the positive integer

$$r_0 \triangleq \begin{cases} \max\{\lceil \frac{n-l}{l-p} \rceil, 1\}, & p < l, \\ 1, & p = l, \end{cases} \quad (\text{III.8})$$

where  $\lceil a \rceil$  denotes the smallest integer greater than or equal to  $a$ . Note that  $r_0$  is not defined in the case  $p > l$ .

*Theorem 3.3:* The following statements are equivalent:

- 1) (III.1), (III.2) is input and state observable.
- 2) For all  $r \geq r_0$ ,  $\mathcal{Y}_r = 0$  if and only if  $\begin{bmatrix} x_0 \\ \mathcal{E}_{r-1} \end{bmatrix} = 0$ .
- 3) For all  $r \geq r_0$ ,  $\text{rank}(\Psi_r) = n + rp$ .
- 4) There exists  $r \geq r_0$  such that  $\text{rank}(\Psi_r) = n + rp$ .
- 5)  $\text{rank}(\Psi_{n-1}) = n + (n-1)p$ .

Theorem 3.3 shows that (III.1), (III.2) is input and state observable if and only if  $\Psi_r$  has full column rank for all

$r \geq r_0$ . In this case the unique solution of (III.6) is

$$\begin{bmatrix} x_0 \\ \mathcal{E}_{r-1} \end{bmatrix} = \Psi_r^\dagger \mathcal{Y}_r, \quad (\text{III.9})$$

where  $\dagger$  represents the Moore-Penrose generalized inverse

$$\Psi_r^\dagger = (\Psi_r^T \Psi_r)^{-1} \Psi_r^T. \quad (\text{III.10})$$

### B. Exactly Proper Case

Consider the linear discrete-time system

$$x_{k+1} = Ax_k + He_k, \quad (\text{III.11})$$

$$y_k = Cx_k + Ge_k, \quad (\text{III.12})$$

where  $G \in \mathbb{R}^{l \times p}$ , while  $A, H, C, x_k, e_k$ , and  $y_k$  are defined as in (III.1), (III.2). Without loss of generality, we assume  $l \leq n$ ,  $\text{rank}(C) = l > 0$ , and  $\text{rank} \begin{bmatrix} H \\ G \end{bmatrix} = p > 0$ . Due to  $Ge_k$ , the output  $y_k$  is directly affected by  $e_k$  as well as by the past values of  $e_k$ . Therefore, we have

$$\mathcal{Y}_r = \bar{\Psi}_r \begin{bmatrix} x_0 \\ \mathcal{E}_r \end{bmatrix}, \quad (\text{III.13})$$

where  $\mathcal{E}_r$  is defined by (III.3),  $\bar{\Psi}_r \triangleq [\Gamma_r \ \bar{M}_r] \in \mathbb{R}^{(r+1)l \times [n+(r+1)p]}$ , and

$$\bar{M}_r = \begin{bmatrix} G & 0 & \cdots & 0 & 0 \\ CH & G & \cdots & 0 & 0 \\ \vdots & \vdots & \ddots & \vdots & \vdots \\ CA^{r-2}H & CA^{r-3}H & \cdots & G & 0 \\ CA^{r-1}H & CA^{r-2}H & \cdots & CH & G \end{bmatrix}.$$

Furthermore, we have the following definition.

**Definition 3.4:** Let  $r \geq 0$ . Then the *input and state unobservable subspace*  $\bar{\mathfrak{U}}_r$  of (III.11), (III.12) is the subspace

$$\bar{\mathfrak{U}}_r \triangleq \left\{ \begin{bmatrix} x_0 \\ \mathcal{E}_r \end{bmatrix} \in \mathbb{R}^{n+(r+1)p} : \mathcal{Y}_r = 0 \right\}. \quad (\text{III.14})$$

The input and state unobservable subspace is given by  $\bar{\mathfrak{U}}_r = \mathcal{N}(\bar{\Psi}_r)$ . Next, if  $p < l$ , then define

$$\bar{r}_0 \triangleq \lceil \frac{n}{l-p} \rceil - 1. \quad (\text{III.15})$$

Since  $n > l - p$ , it follows that  $\bar{r}_0 \geq 1$ .

**Definition 3.5:** The system (III.11), (III.12) is *input and state observable* if  $\bar{\mathfrak{U}}_r = \{0\}$  for all  $r \geq \bar{r}_0$ .

**Theorem 3.6:** The following statements are equivalent:

- 1) (III.11), (III.12) is input and state observable.
- 2) For all  $r \geq \bar{r}_0$ ,  $\mathcal{Y}_r = 0$  if and only if  $\begin{bmatrix} x_0 \\ \mathcal{E}_r \end{bmatrix} = 0$ .
- 3)  $\text{rank}(\bar{\Psi}_r) = n + (r+1)p$  for all  $r \geq \bar{r}_0$ .
- 4) There exists  $r \geq \bar{r}_0$  such that  $\text{rank}(\bar{\Psi}_r) = n + (r+1)p$ .
- 5)  $\text{rank}(\bar{\Psi}_{n-1}) = n(p+1)$ .

If (III.11), (III.12) is input and state observable, then Theorem 3.6 implies that  $\bar{\Psi}_r$  has full column rank for all  $r \geq \bar{r}_0$ . In this case the unique solution of (III.13) is

$$\begin{bmatrix} x_0 \\ \mathcal{E}_r \end{bmatrix} = \bar{\Psi}_r^\dagger \mathcal{Y}_r, \quad (\text{III.16})$$

where

$$\bar{\Psi}_r^\dagger = (\bar{\Psi}_r^T \bar{\Psi}_r)^{-1} \bar{\Psi}_r^T. \quad (\text{III.17})$$

### IV. INVARIANT ZEROS AND UNOBSERVABLE INPUTS

If a linear system has invariant zeros, then it is not input and state observable, that is  $\mathfrak{U}_r \neq \{0\}$ . In particular, there exists an initial state and a nonzero input such that the output is identically zero. Therefore, it is not possible to exactly reconstruct the initial state and the input vector from the measured output. Nevertheless, we use (III.9) and (III.16) for approximate input reconstruction, although the generalized inverses of  $\Psi_r$  and  $\bar{\Psi}_r$  are no longer given by (III.10) and (III.17). We call this the *approximate input reconstruction method*.

Approximate reconstruction must account for the locations of system transmission zeros in the complex plane relative to the unit disk. If all of the transmission zeros are contained in the open unit disk, then approximate causal reconstruction is possible for sufficiently large data sets and large times  $k$ . On the other hand, if all of the transmission zeros are contained in the complement of the closed unit disk, then approximate noncausal reconstruction is possible for sufficiently large data sets and small times  $k$ . Consequently, if all of the system transmission zeros are contained in either the open unit disk or the complement of the closed unit disk, then approximate noncausal reconstruction is possible for sufficiently large data sets and small times  $k$ . Finally, if at least one transmission zero lies on the unit circle, then approximate reconstruction is not possible since a persistent reconstruction error will corrupt the reconstructed inputs.

Let  $P_r$  denote the orthogonal projector onto  $\mathfrak{U}_r$ , and let  $P_{r\perp}$  denote the orthogonal projector onto  $\mathfrak{U}_r^\perp$ . Therefore, for the strictly proper case we have

$$P_r = \Psi_r \Psi_r^\dagger \quad (\text{IV.1})$$

and similarly for the exactly proper case. We thus have the following definition.

**Definition 4.1:** The *observable state and input* are given by

$$\begin{bmatrix} x_{0,\text{rec}} \\ \mathcal{E}_{r-1,\text{rec}} \end{bmatrix} \triangleq P_r \left( \begin{bmatrix} x_0 \\ \mathcal{E}_r \end{bmatrix} \right), \quad (\text{IV.2})$$

while the *unobservable state and input* are given by

$$\begin{bmatrix} x_{0,\text{unrec}} \\ \mathcal{E}_{r-1,\text{unrec}} \end{bmatrix} \triangleq P_{r\perp} \left( \begin{bmatrix} x_0 \\ \mathcal{E}_r \end{bmatrix} \right). \quad (\text{IV.3})$$

It follows from Definition 4.1 that

$$x_0 = x_{0,\text{rec}} + x_{0,\text{unrec}}, \quad (\text{IV.4})$$

$$\mathcal{E}_{r-1} = \mathcal{E}_{r-1,\text{rec}} + \mathcal{E}_{r-1,\text{unrec}}. \quad (\text{IV.5})$$

Therefore, if the linear system is not input and state observable, then the initial state and input consist of the components  $\begin{bmatrix} x_{0,\text{rec}} \\ \mathcal{E}_{r-1,\text{rec}} \end{bmatrix}$  and  $\begin{bmatrix} x_{0,\text{unrec}} \\ \mathcal{E}_{r-1,\text{unrec}} \end{bmatrix}$ . Therefore, the accuracy of the initial state and input reconstruction depends on the magnitude of the unobservable components  $\begin{bmatrix} x_{0,\text{unrec}} \\ \mathcal{E}_{r-1,\text{unrec}} \end{bmatrix}$ . As

numerical examples show, the reconstructed input  $\mathcal{E}_{r-1,\text{unrec}}$  is small for small and large values of  $k$ , respectively, in a system that has only minimum phase and nonminimum-phase zeros. In both cases the reconstruction process involves a batch-processing algorithm. However, in the nonminimum-phase case, the input estimates have good accuracy only for small values of  $k$ , and thus the input reconstruction is noncausal.

### A. Illustrative Example

To illustrate the unobservable state and input, we consider a minimal realization of the transfer function

$$F(z) = \frac{z-a}{(z-0.2)(z-0.3)(z-0.4)}, \quad (\text{IV.6})$$

where the zero  $a$  is given by  $a = 0.1$ ,  $a = 10$ ,  $a = 1$ , or  $a = -1$ . For the case  $a = 0.1$ , Figure 2 shows that the reconstruction improves asymptotically as  $k$  increases, but is poor for small values of  $k$ . This behavior is characteristic of a minimum-phase zero for which the unobservable component of the input converges to zero. In contrast, for the case  $a = 10$ , Figure 3 shows that the reconstruction degrades asymptotically as  $k$  increases, but is good for small values of  $k$ . This behavior is characteristic of a nonminimum-phase zero for which the unobservable component of the input diverges. Consequently, the input reconstruction is noncausal. For the case  $a = 1$ , Figure 4 shows that the reconstruction is poor for all values of  $k$  since the unobservable component of the input is constant and nonzero. As shown in Figure 5, the same situation occurs for  $a = -1$ , where the unobservable component of the input is oscillating. In both cases, the unobservable component is persistent, and thus the input reconstruction is poor.

## V. APPLICATION TO LONGITUDINAL FLIGHT DYNAMICS

In this section we use the approximate input reconstruction algorithm to estimate the input signals to a longitudinal flight dynamics model. In particular, we estimate the elevator deflection and thrust using measurements of range, altitude, pitch-angle perturbation, and total-velocity perturbation, which are assumed to be available from flight sensors. The matrix  $\Psi_r^\dagger$  is based on the state-space matrices of the flight dynamic model. We consider the linearized F-16 model developed in [16], which provides the state-space matrices  $A$ ,  $B$ ,  $C$ , and  $D$  for both decoupled longitudinal and lateral flight dynamics once the altitude and the total velocity of the aircraft are specified.

For longitudinal case, the state-space form of the F-16 model is

$$\dot{X} = AX + BU, \quad (\text{V.1})$$

$$Y = CX + DU, \quad (\text{V.2})$$

where  $X \triangleq [x \ h \ \theta \ u \ \alpha \ q]^T$ ,  $U \triangleq [\delta T \ \delta e]^T$ , and  $Y \triangleq [x \ h \ u]^T$ . The states are range  $x$  (ft), altitude  $h$  (ft), pitch-angle perturbation  $\theta$  (deg), total-velocity perturbation  $u$  (ft/s), angle of attack  $\alpha$  (deg), and pitch rate  $q$  (deg/s). The inputs are elevator deflection  $\delta e$  from trim

and thrust  $\delta T$ , while the available measurements are  $x$ ,  $h$ , and  $u$ . The matrices  $A \in \mathbb{R}^{6 \times 6}$ ,  $B \in \mathbb{R}^{6 \times 2}$ ,  $C \in \mathbb{R}^{3 \times 6}$ , and  $D \in \mathbb{R}^{6 \times 2}$  are given by

$$A = \begin{bmatrix} 0 & 0 & 0 & 0 & 0 & 1 \\ 0 & 0 & 5 & 3.553e-10 & 0 & 0 \\ 0 & 0 & 0 & 0 & 0 & 0 \\ 0 & 1.080e-04 & -3.217e+01 & -1.328e-02 & 0 & 0 \\ 0 & 2.076e-06 & 2.547e-13 & -2.553e-04 & 0 & 0 \\ 0 & 2.573e-20 & 0 & -3.163e-18 & 0 & 0 \\ 0 & 0 & 0 & 0 & 0 & 0 \\ -5.000e+2 & 0 & 0 & 0 & 0 & 0 \\ 0 & 1 & 0 & 0 & 0 & 0 \\ -7.326 & -1.196 & 0 & 0 & 0 & 0 \\ -6.398e-01 & 9.378e-01 & 0 & 0 & 0 & 0 \\ -1.568 & -8.791e-01 & 0 & 0 & 0 & 0 \end{bmatrix}, \quad (\text{V.3})$$

$$B = \begin{bmatrix} 0 & 0 \\ 0 & 0 \\ 0 & 0 \\ 1.565e-03 & 7.397e-02 \\ -2.445e-07 & -1.357e-03 \\ 0 & -1.137e-01 \end{bmatrix}, \quad (\text{V.4})$$

$$C = \begin{bmatrix} 1 & 0 & 0 & 0 & 0 & 0 \\ 0 & 1 & 0 & 0 & 0 & 0 \\ 0 & 0 & 1 & 0 & 0 & 0 \end{bmatrix}, \quad D = 0. \quad (\text{V.5})$$

For the system (V.1)–(V.5), we apply the approximate input reconstruction method. The condition number of  $\Psi_r$  is  $2.8901e+11$  for  $r = 100$ . We obtain the state-space matrices for the trim condition at an altitude of 15,000 ft with a velocity of 500 ft/s. The initial state is thus set to be  $x_0 = [0 \ 15000 \ 0 \ 500 \ 0 \ 0]^T$ . The thrust command  $\delta T$  is chosen to be a constant, and the elevator deflection command  $\delta e$  is chosen to be sinusoidal. Since  $D = 0$ , the unknown commands are estimated using (IV.2) for  $r = 100$ .

Figure 6 shows the commanded inputs and their estimates, including both the observable and unobservable components. The unobservable component is close to zero, which is consistent with the observation that the system is input and state observable.

Using Table 3, fault detection is conducted for a scenario in which the engine is given two successive step commands, while the elevator becomes stuck at  $t = 45$  s. We use the same initial state, commanded inputs, and step command, as above. Figure 7 shows commanded inputs, measured inputs from the linkage sensor and estimated inputs both before and after the fault occurs. The numerical results suggest that Case 4 in Table 3 is applicable.

Alternatively, we assume that  $x$ ,  $h$ , and  $\theta$  are the available outputs, and thus

$$C = \begin{bmatrix} 1 & 0 & 0 & 0 & 0 & 0 \\ 0 & 1 & 0 & 0 & 0 & 0 \\ 0 & 0 & 1 & 0 & 0 & 0 \end{bmatrix}. \quad (\text{V.6})$$

The condition number of  $\Psi_r$  is  $2.6326e+14$  for  $r = 100$ . With the same initial state and commands, Figure 8 shows the the unknown commanded inputs and their estimated inputs. The unobservable component is large, indicating the presence of an invariant zero near the unit circle.

## VI. APPLICATION TO NONMINIMUM PHASE, EXACTLY PROPER FLIGHT DYNAMICS

We now consider a nonminimum-phase flight example, in which the dynamics are exactly proper. We require an inertial Earth frame  $F_E$  with an arbitrary origin, whose axes  $\hat{i}_E$  and  $\hat{j}_E$  are horizontal, and whose axis  $\hat{k}_E$  points downward. The aircraft frame is fixed to the body of the aircraft, and its origin  $O_{AC}$  is located at the aircraft center of mass  $c$ . The frame origin is  $O_{AC}$ , while the frame vectors are  $\hat{i}_{AC}$  and  $\hat{k}_{AC}$ .

We assume that an accelerometer is installed at the location  $p$  on the aircraft in order to measure acceleration  $\hat{a}_{pz}$  in the direction  $\hat{k}_{AC}$ . The position vector from the aircraft center of mass  $c$  to  $p$  is  $\hat{l}_{AC}$ , and thus  $|l|$  is the distance from the aircraft center of mass  $c$  to  $p$ . For a typical business jet with velocity of 675.12 ft/s at an altitude of 4000 ft [17], it can be verified from aircraft kinematics that the trim condition is open-loop stable and that the transfer function from the output of the accelerator to the elevator deflection input is

$$G_{\hat{a}_{pz}/\delta e}(s) = \frac{\hat{a}_{cz}(s)}{\delta e(s)} \quad (\text{VI.1})$$

$$= -\frac{(42.14 - 17.65l)s^4 + (11923.70 - 26.11l)s^3 + (88.46 - 0.12l)s^2 + 79.20s}{s^4 + 2.01074s^3 + 8.04799s^2 + 0.084973s + 0.067893}.$$

This system is nonminimum phase as long as  $l < 276$ . In addition, the dynamics are exactly proper case except when the coefficient of the highest order of  $s$  in the transfer function equals zero, which occurs when  $l = 2.388$ .

To apply approximate input reconstruction to fault detection, we assume that the elevator command is a square wave and that the elevator becomes stuck. The elevator deflection is estimated using (III.16) for  $r = 100$ . The measured output is the acceleration in the direction  $\hat{k}_{AC}$ . Figures 9 and 10 show the unknown deflection inputs and their estimates with  $l$  chosen to be 50 and 274, respectively. It can be seen that, for  $l = 50$ , the unobservable component of the input is close to zero, whereas, for  $l = 274$ , the unobservable component increases with time, which is consistent with the fact that the aircraft dynamics have a nonminimum-phase zero.

## VII. CONCLUSIONS

As an extension of exact input reconstruction, we considered an approximate input reconstruction method where a least squares solution is used in the presence of zeros. For plants with minimum-phase zeros, the input-reconstruction error decays; for nonminimum-phase zeros it grows; and for zeros on the unit circle, it is persistent. We applied this technique to aircraft fault detection, where the objective is to compare the estimated input with the commanded input and the linkage sensor. This comparison provides a technique for online fault detection. We demonstrated the technique for both lateral and longitudinal dynamics, as well as nonminimum-phase exactly proper dynamics. Future work will focus on the effect of model errors and sensor noise on the fault-detection accuracy.

## REFERENCES

- [1] R. K. Douglas and J. I. Speyer. Robust fault detection filter design. *Proc. Amer. Contr. Conf.*, 91–96, 1995.
- [2] R. Isermann, *Fault Detection and Diagnosis in Engineering Systems*. CRC, 1998.
- [3] R. Isermann, *Fault Diagnosis Systems: An Introduction from Fault Detection to Fault Tolerance*. Springer, 2005.
- [4] M. Blanke, M. Kinnaert, J. Lunze, and M. Saroswiecki, *Diagnosis and Fault-Tolerant Control*. Springer, 2006.
- [5] J.L. Massey and M.K. Sain. Inverses of linear sequential circuits. *IEEE Transactions of Automatic Control*, C-17:330–337, 1968.
- [6] M. K. Sain and J. L. Massey. Invertibility of linear time-invariant dynamical systems. *IEEE transactions on automatic control*, AC-14:141–149, 1969.
- [7] M. Tomizuka. Zero phase error tracking algorithm for digital control. *ASME Journal of Dynamic Systems, Measurement, and Control*, 109:65–68, 1987.
- [8] E. Gross and M. Tomizuka. Experimental flexible beam tip tracking control with a truncated series approximation to uncancellable inverse dynamics. *IEEE transactions on control systems technology*, 2:382–391, 1994.
- [9] E. Gross, M. Tomizuka, and W. Messner. Cancellation of discrete time unstable zeros by feedforward control. *Journal of Dynamic Systems, Measurement, and Control*, 116:33–38, 1994.
- [10] J. Chen, R. J. Patton, and H.-Y. Zhang. Design of unknown input observers and robust fault detection filters. *Int. J. Contr.*, 63:85–105, 1996.
- [11] G. Marro, D. Prattichizzo, and E. Zattoni, “A unified algorithmic setting for signal-decoupling compensators and unknown-input observers,” *Proc. Conf. Dec. Contr.*, pp. 4512–4517, Sydney, Australia, 2000.
- [12] G. Marro, D. Prattichizzo, and E. Zattoni, “Convolution profiles for right inversion of multivariable non-minimum phase discrete-time systems,” *Automatica*, Vol. 38, pp. 1695–1703, 2002.
- [13] S. Gillijns. *Kalman Filtering Techniques for System Inversion and Data Assimilation*. PhD thesis, 2007.
- [14] J. A. Butterworth, L. Y. Pao, and D. Y. Abramovitch. The effect of nonminimum-phase zero locations on the performance of feedforward model-inverse control techniques in discrete-time systems. *2008 American Control Conference*, 2008.
- [15] H. J. Palanthandlam-Madapusi and D. S. Bernstein, A Subspace Identification Algorithm for Simultaneous Identification and Input Reconstruction. *Proc. Conf. Dec. Contr.*, pp. 4956–4961, New Orleans, LA, December, 2007; *Int. J. Adapt. Control Signal Process*, to appear.
- [16] R. S. Russell, Non-linear F-16 Simulation using Simulink and Matlab, June, 2003. <[http://www.aem.umn.edu/people/faculty/balas/darpa\\_sec/software](http://www.aem.umn.edu/people/faculty/balas/darpa_sec/software)>.
- [17] J. Roskam, *Airplane Flight Dynamics and Automatic Flight Controls*. DARcorporation, 2001.

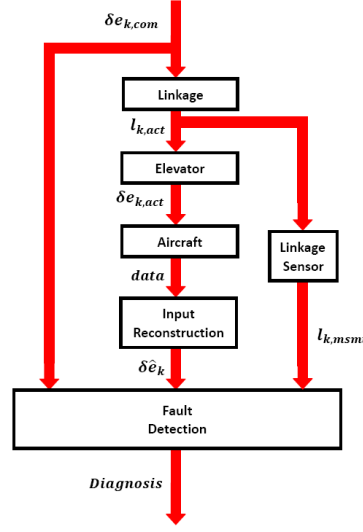


Fig. 1. Signals used for elevator fault detection

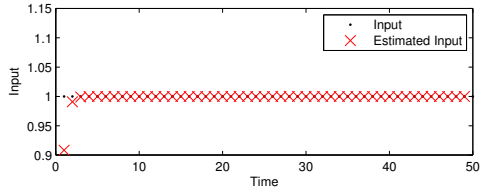


Fig. 2. Example (IV.6) with minimum phase zero  $a = 0.1$ . The unobservable component is close to zero except for small values of  $k$ .

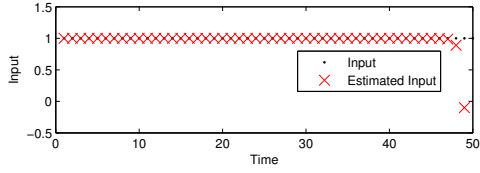


Fig. 3. Example (IV.6) with nonminimum-phase zero  $a = 10$ . The unobservable component is close to zero except for large values of  $k$ .

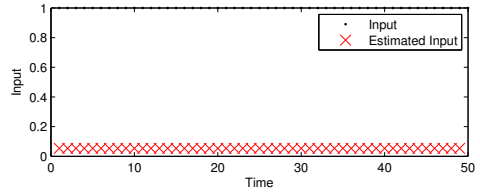


Fig. 4. Example (IV.6) with zero  $a = 1$  on the unit circle. In this case, the reconstructed input has a persistent component.

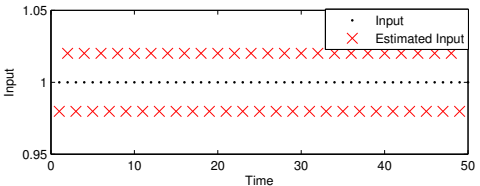


Fig. 5. Example (IV.6) with zero  $a = -1$  on the unit circle. In this case, the reconstructed input has a persistent component.

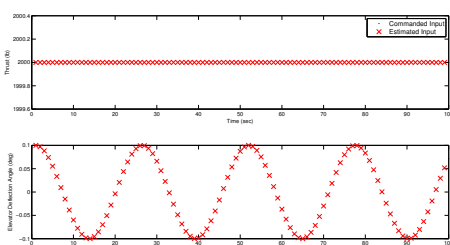


Fig. 6. Input reconstruction for F-16 longitudinal flight. Estimates of the unknown inputs  $\delta T$  and  $\delta e$  are obtained by using measurements of the outputs  $x$ ,  $h$ , and  $u$  and the linearized flight model. In this case, the unobservable input is close to zero.

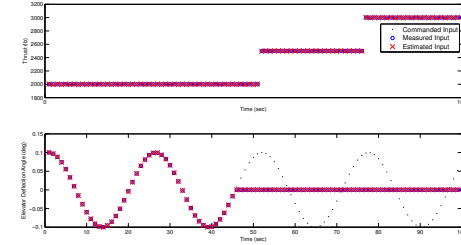


Fig. 7. Input reconstruction for F-16 longitudinal flight. Estimates of the unknown inputs  $\delta T$  and  $\delta e$  are obtained by using measurements of the outputs  $x$ ,  $h$ , and  $u$  and the linearized longitudinal flight model. For this example, the input reconstruction algorithm and the logic of Table 4 indicate that the engine is operational, whereas the elevator is stuck.

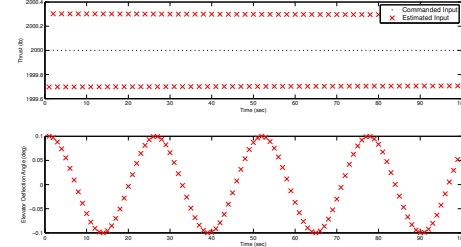


Fig. 8. Input reconstruction for F-16 longitudinal flight. Estimates of the unknown inputs  $\delta T$  and  $\delta e$  are obtained by using measurements of the outputs  $x$ ,  $h$ , and  $u$  and the linearized flight model. In this case, the unobservable input is not close to zero, suggesting the presence of an invariant zero near the unit circle.

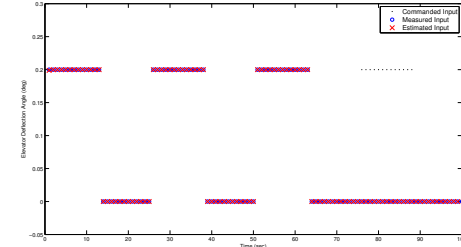


Fig. 9. Nonminimum-phase aircraft example with forward-mounted accelerometer. For this example, the distance from the aircraft center of mass to the accelerometer is  $l = 50$  ft. The output is  $\hat{a}_{cz}$ , while  $\delta e$  is the input. Both observable and unobservable components are shown. Note that the unobservable component is close to zero, which indicates the absence of zeros near the unit circle.

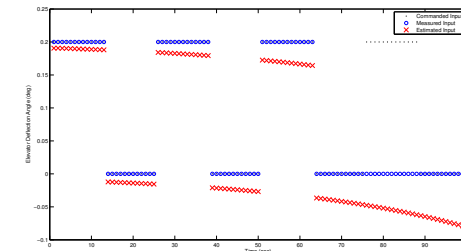


Fig. 10. Nonminimum-phase aircraft example with forward-mounted accelerometer. For this example, the distance from the aircraft center of mass to the accelerometer is  $l = 275$  ft. The output is  $\hat{a}_{cz}$ , while  $\delta e$  is the input. Both observable and unobservable components are shown. Note that the unobservable component is large for large  $k$ , which indicates the presence of a nonminimum-phase zero close to the unit circle.